Nanoscale Res Lett (2009) 4:814–819
DOI 10.1007/s11671-009-9320-z

NANO EXPRESS

SiC Nanorods Grown on Electrospun Nanofibers Using Tb as Catalyst: Fabrication, Characterization, and Photoluminescence Properties

Jin-Yuan Zhou · Zhi-Yong Chen · Ming Zhou · Xiu-Ping Gao · Er-Qing Xie

Received: 2 March 2009 / Accepted: 6 April 2009 / Published online: 15 May 2009

Abstract Well-crystallized β-SiC nanorods grown on electrospun nanofibers were synthesized by carbothermal reduction of Tb doped SiO_2 (SiO_2:Tb) nanofibers at 1,250 °C. The as-synthesized SiC nanorods were 100–300 nm in diameter and 2–3 μm in length. Scanning electron microscopy (SEM) results suggested that the growth of the SiC nanorods should be governed by vapor-liquid-solid (VLS) mechanism with Tb metal as catalyst. $Tb(NO_3)_3$ particles on the surface of the electrospun nanofibers were decomposed at 500 °C and later reduced to the formation of Tb nanoclusters at 1,200 °C, and finally the formation of a Si–C–Tb ally droplet will stimulate the VLS growth at 1,250 °C. Microstructure of the nanorod was further investigated by transmission electron microscopy (TEM). It was found that SiC <111> is the preferred initial growth direction. The liquid droplet was identified to be $Si_{86}Tb_{14}$, which acted as effective catalyst. Strong green emissions were observed from the SiC nanorod samples. Four characteristic photoluminescence (PL) peaks of Tb ions were also identified.

Keywords SiC nanorods · Vapor-liquid-solid mechanism · Terbium · Electrospinning · Photoluminescence

J.-Y. Zhou · Z.-Y. Chen · M. Zhou · X.-P. Gao · E.-Q. Xie (✉)
Key Laboratory for Magnetism and Magnetic Materials of the Ministry of Education, Lanzhou University, 222 South Tianshui Road, Lanzhou, 730000 Gansu, People's Republic of China
e-mail: xieeq@lzu.edu.cn

J.-Y. Zhou
e-mail: zhoujy@lzu.edu.cn

Introduction

SiC nanomaterials have promising applications in electronics and photonics owing to their attractive optical, electrical, mechanical, and thermal properties [1]. In particular, SiC nanorods have excellent mechanical and field emission properties, which find potential applications in various nanocomposite materials and in field emission nanoscale devices [2–4].

Since the first synthesis of carbide nanorods using carbon nanotube as templates by Dai group [5], SiC nanorods have been successfully synthesized by various methods. Vapor-liquid-solid (VLS) growth mechanism is one of the methods that have been extensively employed [6–10]. VLS mechanism was first developed by Wagner and Ellis for the growth of silicon whiskers [11]. The primary feature of VLS mechanism is that the liquid metal alloy droplets sit on the tip of the nanorods and act as the catalyst for the continued growth of the nanorods. For SiC nanorods, Fe, Co, Ni, and Al metals are the most common catalysts used in the VLS process [3, 4, 6, 8–10]. Most of these metals used as catalyst can stimulate only the growth of the nanostructures, but not affect the properties of the samples. Recently, rare earth Tb was used as a catalyst for the growth of GaN nanowires [12].

In this study, SiC nanorods were synthesized through the conventional carbothermal reduction of electrospun SiO_2:Tb nanofibers. The as-grown SiC nanorods possess unique morphologies and show good properties. It is concluded that Tb is a good catalyst for the growth of SiC nanorods. Growth mechanism and PL properties of the Tb doped SiC nanorods were mainly discussed.

Experimental

First, SiO_2:Tb nanofibers were prepared by electrospinning technique [13]. 1 ml of tetraethyl orthosilicate ($SiO_2 \geq$ 28%), 3 ml of ethanol (≥99.7%), 0.5 g of polyvinyl pyrolidone (PVP) (Sigma–Aldrich, *M*w ≈ 1,300,000), 0.03 g of $Tb(NO_3)_3 \cdot 6H_2O$, 0.5 ml of acetic acid, and 0.5 ml of *N*, *N*-dimethyl formamide (DMF) were dissolved together into one mixture. This work was performed under a strong magnetic stirring. After stirred for 2 h, the mixture was sent to an improved electrospinning setup, which was equipped with a heating capability. Then a voltage of 12 kV and a distance of 21 cm were set to the experimental setup. After spinning, SiO_2:Tb nanofibers were collected on a clean silicon wafer in the air. Finally, the as-spun samples were pretreated at 1,200 °C in a close round alumina crucible with a graphite inwall, i.e., a carbothermal environment, for 1 h, and then annealed at 1,250 °C for another hour.

The as-synthesized samples were characterized and studied by X-ray diffraction (XRD, Philips, X'pert Pro, Cu K_α, 0.154056 nm.), field-emission scanning electron microscopy (FE-SEM, Hitachi S-4800), and transmission electron microscopy (TEM, JEOL JEM-2010), equipped with selected area electron diffraction (SAED) and energy dispersive spectroscopy (EDS). The micro-PL and micro-Raman spectra of the samples were obtained by using a micro-Raman spectroscopy (JY-HR800, 325 nm exciting source of a He–Cd laser).

Results and Discussion

Figure 1 shows the XRD pattern and micro-Raman spectrum of the SiC nanorod samples annealed at 1,250 °C for 1 h. The four strong diffraction peaks in Fig. 1a correspond to the (111), (200), (220), and (311) planes of β-SiC (JCPDS, No. 29-1129), respectively. An additional diffraction peak marked with a star may be due to the stacking faults in the samples [7]. One can see from the Raman spectrum (Fig. 1b) that, apart from the D- and G- peaks of graphite at 1367 and 1610 cm^{-1}, there are three distinct peaks of SiC at 756, 800, and 910 cm^{-1}, respectively. According to Peng et al. [14], the peaks at 765 and 800 cm^{-1} correspond to the TO modes of β-SiC, while the peak at 910 cm^{-1}, with about 50 cm^{-1} Raman redshift, may be due to the LO mode of a mixture of Si–C–Tb compositions or a high density of stacking faults within the samples. In addition, the SiC nanostructures themselves in this case may also contribute to the shift of Raman peaks due to the size effect.

SEM images show a high-yield and unique morphology of the nanorods grown on the precursor nanofibers at the temperature of 1,250 °C. As shown in Fig. 2a, most of the nanorods are straight with length up to 2–3 μm and diameter ranging from 100 nm to 300 nm. The corresponding growth rate is 2–3 μm/h, which is close to the previous good results [4]. Figure 2b displays a higher magnification SEM image of the nanorods. The nanorods are straight with spherical particles at their tips, which is a typical phenomenon of VLS type of growth. It is suggested that the growth of these SiC nanorods may take place by means of the VLS mechanism [11].

More detailed SEM analyses revealed the morphological evolution of the SiC nanorods as a function of temperature. Figure 3a is a typical SEM image of the as-spun SiO_2:Tb nanofibers. The surface of the fibers is smooth and uniform without any particle. After annealing at 1,200 °C for

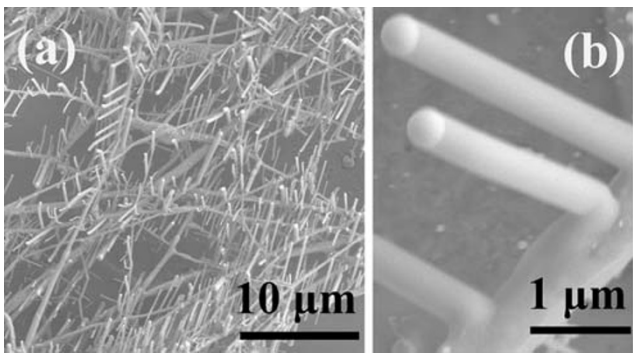

Fig. 2 SEM images of the SiC nanorods: (**a**) low magnification, and (**b**) high magnification

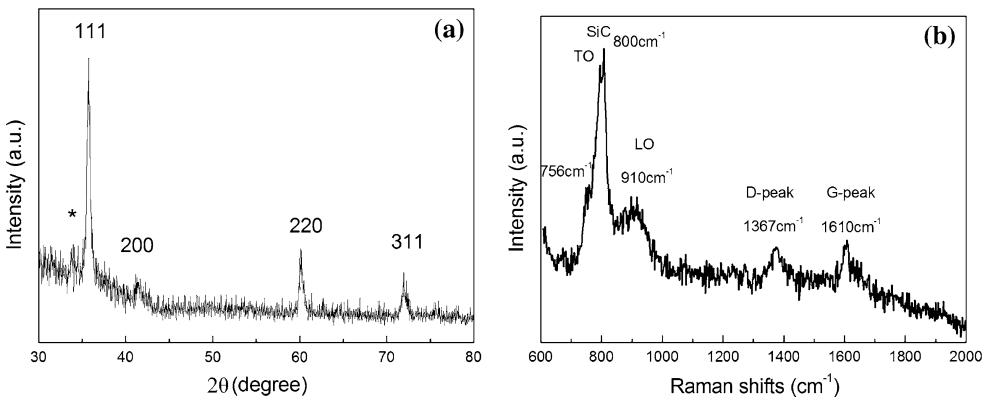

Fig. 1 **a** XRD pattern and **b** micro-Raman spectrum of the SiC nanorod samples annealed at 1,250 °C for 1 h

60 min, many white spots will appear on the surface of the nanofibers, as shown in Fig. 3b. Further annealing at 1,250 °C for 60 min, long, straight, and round-ended SiC nanorods will grow on the surface of the nanofibers, as shown in Fig. 3c. So, a schematic graph can be drawn at the bottom of Fig. 3 showing the growth process of the SiC nanorods. The whole growth process can be generally described as follows:

$$2\mathrm{Tb(NO_3)_3} \xrightarrow{>500^\circ\mathrm{C}} \mathrm{Tb_2O_3} + 3(\mathrm{N_2O_5})\uparrow, \quad (1)$$

$$\mathrm{Tb_2O_3} + 3CO\uparrow \xrightarrow{>1100^\circ\mathrm{C}} 2Tb + 3CO_2\uparrow, \quad (2)$$

$$SiO_2 + CO \xrightarrow{>1200^\circ\mathrm{C}} SiO\uparrow + CO\uparrow, \quad (3)$$

$$SiO\uparrow + 3CO \xrightarrow{SiTb_x,1250^\circ\mathrm{C}} SiC + 2CO_2\uparrow. \quad (4)$$

$Tb(NO_3)_3$ particles on the sample surface were decomposed at 500 °C in the air and reduced by the high-concentration carbon monoxide to form Tb nanoclusters (the spots on the surface of the nanofibers) at 1,200 °C in a carbothermal environment. And then, Tb nanoclusters would absorb silicon atoms from the feed gas to form Si–Tb alloy droplets with a continuous heating, which acted as the catalyst. As seen from the EDS results presented in Fig. 4g, the phase of the Si–Tb alloy in our experiments was $Si_{86}Tb_{14}$, which was close to the phase of $Si_{82}Tb_{18}$ with a melting point of 1,220 °C [15]. Then, the Si–Tb droplets react with carbon monoxide and silicon dioxide in the atmosphere to form a liquid Si–C–Tb alloy at 1,250 °C. Once the liquid alloy become supersaturated with materials necessary for the nanorod growth, nanocrystals will start to grow by precipitation below the liquid droplets, and then the nanorods formed. Finally, the growth terminated with a liquid-like globule left at the tip of the nanorods, as shown in Fig. 3c.

To investigate the initial stages of VLS growth in this case, the annealing time at 1,250 °C was set to 5 min, and

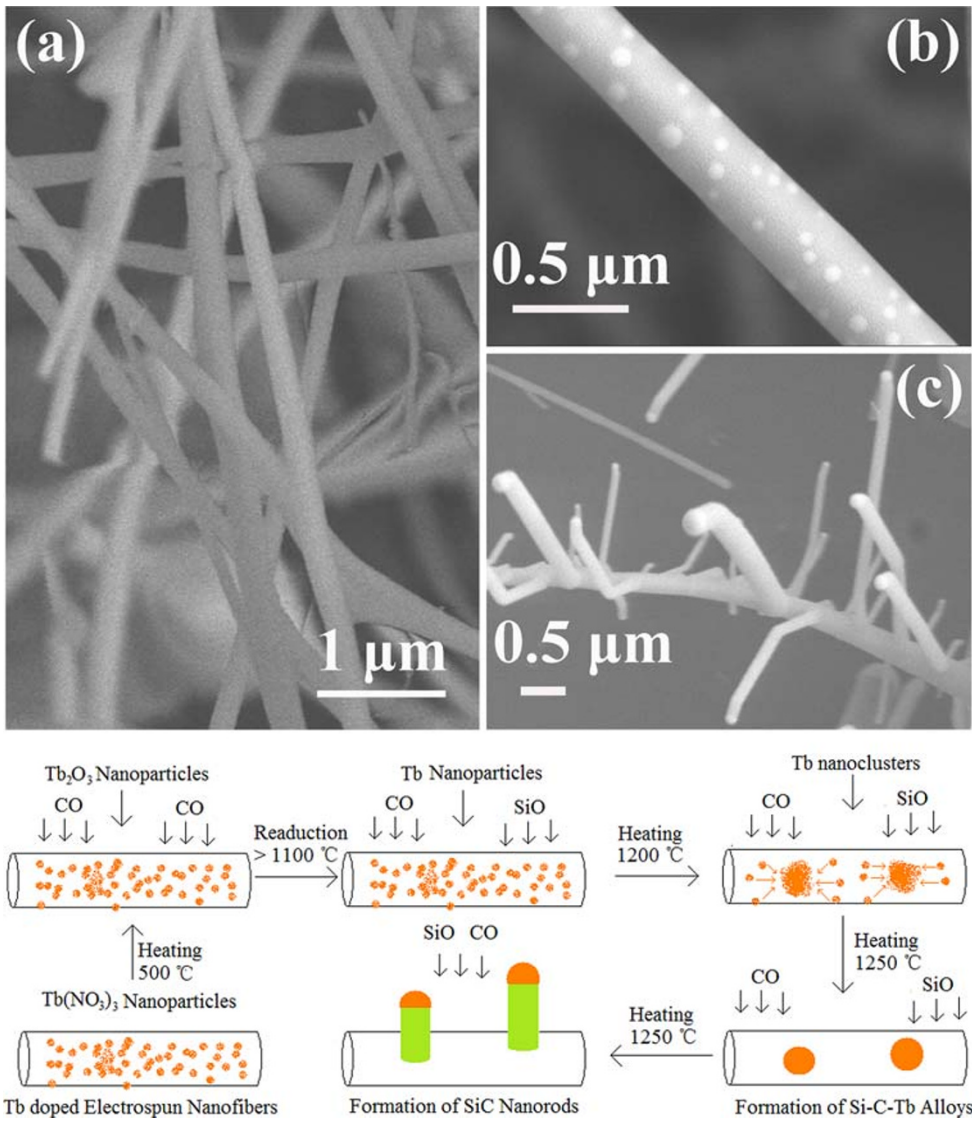

Fig. 3 SEM images of **a** SiO_2 precursor nanofibers, **b** Tb nanoclusters occurring on the surface of the precursor nanofibers at 1,200 °C, and **c** SiC nanorods grown on the precursor nanofibers at 1,250 °C for 1 h. Bottom: Schematic illustration of the VLS growth process of the SiC nanorods grown on the precursor nanofibers

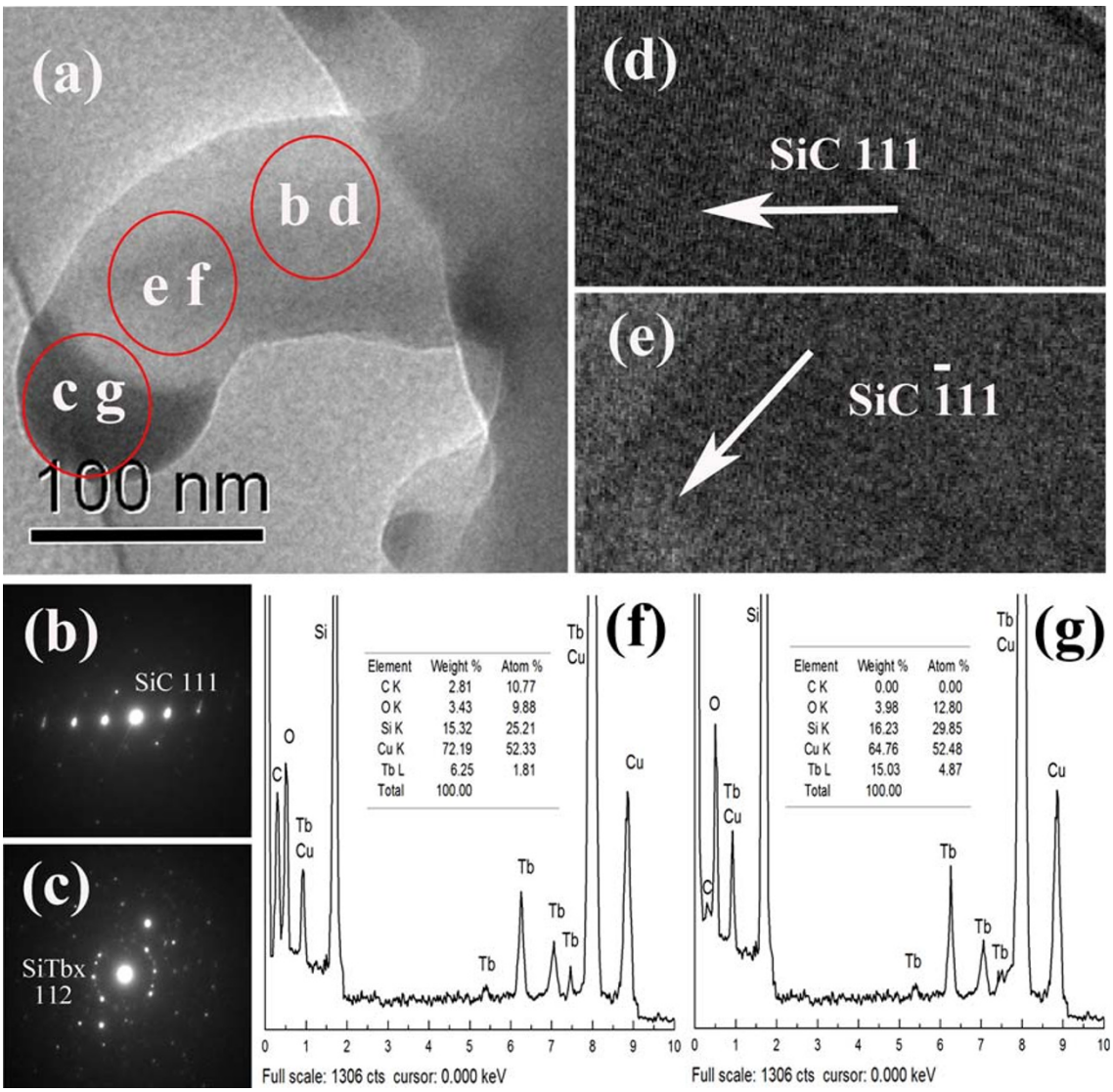

Fig. 4 **a** Low-magnification TEM images of the SiC nanorods annealed at 1,250 °C for 5 min. **b** and **c** SAED patterns recorded from the corresponding areas of SiC nanorod marked in **a**, respectively. **d** and **e** High-magnification TEM lattice image taken from the corresponding areas of the SiC nanorods marked in **a**, respectively. **f** and **g** EDS spectra collected from the corresponding areas marked with circles in **a**, respectively

then TEM was used to reveal the microstructure of the nanorods. Figure 4a is a low-magnification TEM image of a nanorod grown on a nanofiber. The nanorod can be divided into two sections, which indicate two different growth directions of the SiC nanorod. This is similar to the top parts of many nanorods presented in Fig. 3c.

As shown in Fig. 4b and c, SAED patterns indicate that the stem of the nanorod should be well-crystallized β-SiC grown along the <111> direction, which is consistent with the XRD pattern shown in Fig. 1a. The tip of the nanorod should consist of a mixture of Si–Tb compositions, which may attribute to the large Raman shift of LO modes of β-SiC shown in Fig. 1b. The brightest diffraction spot in Fig. 4b corresponds to the SiC <111> direction, while the diffraction ring made up of many small spots may be caused by $SiTb_x$ compounds in the tip of SiC nanorod. Based on the ED spots, the lattice constants can be calculated as 0.3885 and 0.4121 nm, respectively, which are smaller than that of SiC or Si. Referred to the lattice constants 0.3739 nm of $TbFe_2SiC$ (JCPDS, No. 47-1093) and 0.4036 nm of Si_2Tb (JCPDS, No. 13-0383), it can be suggested that the terbium atoms have penetrated into the SiC lattice, and the end-tip of the nanorod consists of Si–Tb compounds.

High-magnification TEM images of the SiC nanorods (as shown in Fig. 4d and e) indicate that SiC <111> is the preferred growth direction at the initial stage of the VLS growth of SiC nanorods [14]. After the initial growth, if temperature is changed around the growth front of the

nanorod, a different growth direction may be selected, and the growth orientation may switch to another SiC <111>, such as $<\bar{1}11>$ [16]. This is similar to the VLS growth of silicon whiskers [17]. In our experiments, once the annealing was terminated, the VLS growth could not stop immediately, and the actual growth condition for the VLS mechanism was changed that resulting in a change of the growth direction and the formation of stacking faults in the samples. This is why most of SiC nanorods shown in Fig. 3c are wry-necked.

Figure 4f and g are EDS spectra collected from the marked areas in Fig. 4a. It can be observed that, leaving out account of Cu from copper TEM grid, the atomic components of the stem and the end-tip of SiC nanorod are $Si_{52.88}C_{22.60}$ $O_{20.72}Tb_{3.80}$ and $Si_{62.82}$ $O_{26.93}Tb_{10.25}$, respectively. These results suggest that the Tb atoms should be homogeneously doped into the SiC nanorods, which is consistent with our analysis of the SAED patterns.

As mentioned in the introduction, the PL properties of the materials were improved by Tb doping in SiC nanorods. Figure 5 compares the room temperature micro-PL spectra of two Tb doped SiC (SiC:Tb) samples. The PL spectrum taken from the SiC:Tb films, which were prepared from the same sol–gel solution, exhibit a weak fluorescence emission band, with the similar profile to the previous results [18], centered at 550 nm. While the SiC:Tb nanorods generate a much stronger fluorescence emission with four characteristic emission transitions of the Tb ions. The peaks at 488, 545, 585, and 620 nm are attributed to the intra-4f $^5D_4 \rightarrow {}^7F_j$ transitions ($j = 6, 5, 4, 3$) of Tb ions [19], respectively. The strongest peak at 545 nm, splitting into two lines (543 nm and 547 nm), is assigned to the $^5D_4 \rightarrow {}^7F_5$ transitions. According to Chen group [20], the weaker wave packet at about 425 nm may be related to the band-gap and defect-related emissions of SiC nanorods.

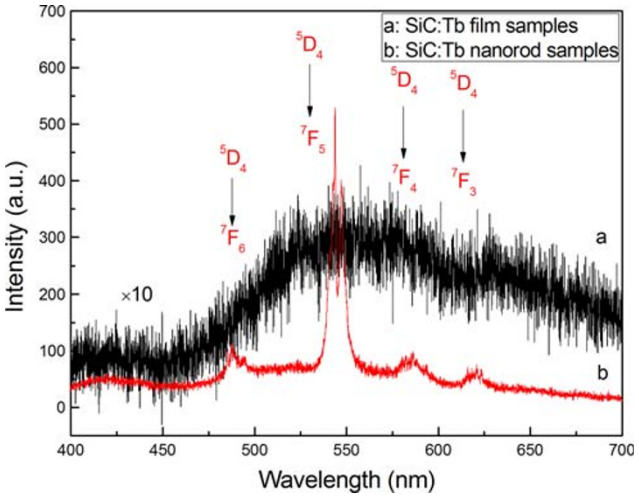

Fig. 5 Micro-PL spectrum of the Tb doped SiC nanorod and film samples annealed at 1,250 °C for 1 h

So far, the emission mechanism of rare earth doped SiC materials is still unclear. Moreover, the most investigated rare earth doping into SiC materials has been focused on erbium (Er). Markmann and Uekusa groups have found that the oxygen impurities can enhance the PL intensity of Er doped SiC materials [21, 22]. Moreover, Gallis group found that the PL intensity of Er doped SiC material depends on the carbon and oxygen content [23]. The strongest PL was observed from the *a*-$SiC_{0.53}O_{0.99}$: Er samples, which are quite similar to our samples $Si_{52.88}C_{22.60}$ $O_{20.72}Tb_{3.80}$. As to rare earth Tb doping, Xu group have suggested that the oxygen-deficiency centers (ODCs) should contribute to the PL of the doped SiC material [24]. Therefore, combining the previous research, it can be suggested that the Si–C–O compositions have great influence on the enhancement of the green light emission from SiC_xO_y:Tb nanorods. Furthermore, the unique structure and the quantum confinement effect coming from the nanostructures may also contribute to the PL enhancement of the samples [3, 4].

Conclusions

In summary, well-crystallized β-SiC nanorods grown on the SiC nanofibers were synthesized through a VLS process with Tb as the catalyst. The nanorods prepared under a particular process are most straight and long, up to 2–3 μm, with a diameter ranging from 100 to 300 nm. SiC <111> is the preferred growth direction at the initial stage. Once the growth conditions change, the next growth will change to another <111> direction. The effective catalyst in our experiments is $Si_{86}Tb_{14}$. The EDS and PL results showed that the Tb atoms have diffused into the SiC matrix, and a high-concentration of oxygen impurities in the samples have enhanced the green light emission of SiC_xO_y:Tb nanorods. The unique structure of the samples and the dopant of rare earth greatly enhanced the PL of the SiC material. This indicates that the rare earth dopant will make the SiC nanostructures good candidates for more photoelectric applications.

Acknowledgments This work was financially supported by the Program for New Century Excellent Talents in University of China (Grant No: NCET-04-0975), and partially by the Natural Science Foundation of Gansu Province in China (Grant No: 0710RJZA041). In addition, the authors thank Dr. H.-P. Sun from University of Michigan for helpful suggestion of the manuscript.

References

1. J.Y. Fan, X.L. Wu, P.K. Chu, Prog. Mater. Sci. **51**, 983 (2006). doi:10.1016/j.pmatsci.2006.02.001
2. E.W. Wong, P.E. Sheehan, C.M. Lieber, Science **277**, 1971 (1997). doi:10.1126/science.277.5334.1971

3. S.Z. Deng, Z.B. Li, W.L. Wang, N.S. Xu, J. Zhou, X.G. Zheng, H.T. Xu, J. Chen, J.C. She, Appl. Phys. Lett. **89**, 023118 (2006). doi:10.1063/1.2220481
4. H.L. Lai, N.B. Wong, X.T. Zhou, H.Y. Peng, F.C.K. Au, N. Wang, I. Bello, C.S. Lee, S.T. Lee, X.F. Duan, Appl. Phys. Lett.**76**, 294 (2000). doi:10.1063/1.125636
5. H.J. Dai, E.W. Wong, Y.Z. Lu, S.S. Fan, C.M. Lieber, Nature **375**, 796 (1995). doi:10.1038/375769a0
6. G. Ferro, C. Jacquier, New J. Chem. **28**, 889 (2004). doi:10.1039/b316410c
7. G. Shen, Y. Bando, C. Ye, B. Liu, D. Golberg, Nanotechnology **17**, 3468 (2006). doi:10.1088/0957-4484/17/14/019
8. T. Seeger, P.K. Redlich, M. Rühle, Adv. Mater. **12**, 279 (2000). doi:10.1002/(SICI)1521-4095(200002)12:4<279:AID-ADMA279>3.0.CO;2-1
9. Z. Li, W. Gao, A. Meng, Z. Geng, L. Wan, J. Cryst. Growth **310**, 4401 (2008). doi:10.1016/j.jcrysgro.2008.06.023
10. S.Z. Deng, Z.S. Wu, J. Zhou, N.S. Xu, J. Chen, J. Chen, Chem. Phys. Lett. **364**, 608 (2002). doi:10.1016/S0009-2614(02)01336-2
11. R.S. Wagner, W.C. Ellis, Appl. Phys. Lett. **4**, 39 (1964). doi:10.1063/1.1753975
12. J. Chen, C. Xue, H. Zhuang, L. Qin, H. Li, Z. Yang, Appl. Surf. Sci. **254**, 4716 (2008). doi:10.1016/j.apsusc.2008.01.083
13. D. Li, Y. Xia, Adv. Mater. **16**, 1151 (2004). doi:10.1002/adma.200400719
14. H.Y. Peng, X.T. Zhou, H.L. Lai, N. Wang, S.T. Lee, J. Mater. Res. **15**, 2020 (2000). doi:10.1557/JMR.2000.0290
15. H. Okamoto, J. Phase Equil. **21**, 500 (2000). doi:10.1361/105497100770339824
16. G. McMahon, G.J.C. Carpenter, T.F. Malis, J. Mater. Sci. **26**, 5655 (1991). doi:10.1007/BF02403970
17. R.S. Wagner, US Patent 4393431 (1970)
18. M. Sendova-Vassileva, M. Nikolaeva, D. Dimova-Malinovska, M. Tzolov, J.C. Pivin, Mater. Sci. Eng. B **81**, 185–187 (2001). doi:10.1016/S0921-5107(00)00734-0
19. H. Amekura, A. Eckau, R. Carius, C. Buchal, J. Appl. Phys. **84**, 3867 (1998). doi:10.1063/1.368591
20. Z. Chen, Y. Wang, Y. Zou, J. Wang, Y. Li, H. Zhang, Appl. Phys. Lett. **89**, 141913 (2006). doi:10.1063/1.2360231
21. M. Markmann, E. Neufeld, A. Sticht, K. Brunner, G. Abstreiter, C. Buchal, Appl. Phys. Lett. **75**, 2584 (1999). doi:10.1063/1.125085
22. S. Uekusa, K. Awahara, M. Kumagai, IEEE Trans. Electron. Dev. **46**, 572 (1999). doi:10.1109/16.748879
23. S. Gallis, M. Huang, H. Efstathiadis, E. Eisenbraun, A.E. Kaloyeros, E.E. Nyein, U. Hommerich, Appl. Phys. Lett. **87**, 091901 (2005). doi:10.1063/1.2032600
24. D.Y. Xu, Y.P. Liu, Z.Y. Chen, Z.W. He, X.Q. Liu, Y.Y. Wang, Mater. Sci. Forum **475–479**, 3681 (2005). doi:10.4028/www.scientific.net/MSF.475-479.3681